

# Numerical simulation of flow through 2-D channel with constriction using OpenFOAM

**Syed Aaqib Ahmed A**

Sr. Design Engineer, TTCADD, Vellore – India

Email: [syedaaqibahmeda@gmail.com](mailto:syedaaqibahmeda@gmail.com)

## Abstract

This report aims to present the characteristics of air flow through channel with constriction. The geometry of the flow channel is of 2m long with 0.1m x 0.01m. The span of constriction considered is 0.01m. For the analysis, the three geometry (0.01m, 0.02m and 0.03m) of the constriction are evaluated. Both the geometry and the mesh are developed and generated using the blockMesh utility of the OpenFoam V-12. The generated mesh is simple-graded. The simulations are carried out using the icoFoam solver, which is a transient laminar flow solver. The analysis are conducted for three Reynolds number conditions of  $Re = 20, 100$  and  $200$ . Accordingly, there are nine simulations. The velocity at the constriction, before the constriction and after the constriction are evaluated. Also, the pressure gradient across the flow is described. The velocity and pressure gradient contours are obtained using the ParaView software. From the analysis, it is observed that with the increase in the span of the constriction, the pressure gradient increases. This increase in the pressure gradient with the increase in the span of constriction is found to be substantial at higher Reynolds number. Further, the velocity profiles and velocity stream lines indicate the recirculation zones, in particular downstream of the constriction. The size of recirculation zones found to increase with Reynolds number and constriction size.

**Keywords:** *flow through constriction, pressure gradient, OpenFoam*

## 1. Introduction

The transportation of fluid through pipes is a commonly observed phenomenon in many applications like petroleum and petrochemical industry and municipal water systems. In such flows, due to corrosion and accumulation of sedimentation, the passage for the fluid flow is reduced. Generally, the accumulation of these sediments initiates with partial reduction of flow passage. For example, in petroleum industry, with the transport of crude oil through pipes, due to sedimentation, corrosion of pipes and accumulation of waxy crude on the pipe wall, the passage for the fluid flow is partially blocked and referred as flow assurance issues. In such a

scenario, the process efficiency and cost are abruptly affected (Ferrante et al. 2014). Accordingly, there have been many investigations to study the characteristics of the fluid flow through pipes with partial blockages (N. M. C. Martins et al 2023; N. M. C. Martins et al 2021). In the literature, characterisation of such phenomenon is also investigated employing the orifices of different sizes in the flow (Hasegawa et al. 1997; Johansen 1997; Kiljanski 1993; Martin et al. 2021; Zhou et al. 2024).

## 2. Problem Statement

In many practical applications, due to the formation of these “partial blockages” and depending on the size of blockages, the pressure waves are found oscillate to and fro along the flow (Meniconi et al. 2018; Keramat et al. 2019). Towards troubleshooting in such situations, the comprehension of velocity and pressure characteristics of the flow with blockages may facilitate. Keeping this in consideration, further comprehension of flow with these partial blockages is required. In the present work, the partial blockages is referred as constrictions – term referred in oil-gas industry.

### 2.1 Objectives and scope of present work

To evaluate the characteristics of a 2D air flow through passage (refer Fig. 1) with constrictions using OpenFoam. In particular, the velocity and pressure characteristics are investigated. The Reynolds number of the flow considered are 20, 100 and 200 (all three case are in laminar regime).

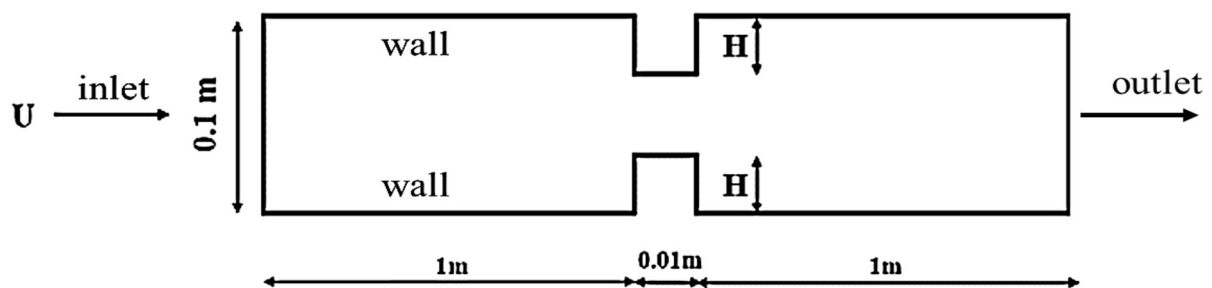


Fig. 1 Flow domain

The size of the constriction is also varied and the values of  $H$  considered are 0.01, 0.02 and 0.03m. Accordingly, the velocity of air determined for these three Reynolds numbers are 0.0032m/s, 0.016m/s and 0.032m/s (refer Table 1 below).

**Table 2.1** Flow conditions

Reynolds number (-)	Flow velocity (m/s)
20	0.0032
100	0.0161
200	0.0322

For the simulation, the kinematic viscosity of air is considered at 30°C as  $1.608 \times 10^{-5} \text{ m}^2/\text{s}$ . The results of the numerical simulation are validated using the experimental data available in the literature.

### 3. Governing Equations

Basically, for the simulation, the conservation equations of mass and momentum are applied. Accordingly, the continuity equation is given as:

$$\frac{\partial \rho}{\partial t} + \nabla \cdot (\rho \cdot U) = 0 \quad (1)$$

Here, the parameters  $S$ ,  $U$ ,  $t$ ,  $\rho$  are source, mean velocity, time and density respectively. Further, the momentum equation of each fluid phase may be considered as:

$$\frac{\partial(\rho U)}{\partial t} + \nabla \cdot (\rho \cdot U \cdot U) = -\nabla P + \nabla \cdot [\mu(\nabla U + \nabla U^T)] + \rho g + F \quad (2)$$

with  $P$ ,  $g$ ,  $\mu$  and  $F$  are referred as pressure gradient across the flow, acceleration due to gravity, viscosity of fluid phases and body forces respectively.

## 4. Creation of Mesh and Simulation

### 4.1 Geometry and Mesh

Since the geometry is simple, the geometry was created using the blockMesh utility of OpenFoam. This utility employs a dictionary file referred as blockMeshDict and this dictionary file is generally placed in the constant/polyMesh directory. Also, the mesh is generated and stored in the same directory as points, faces, internalfaces and cells files. Three blocks are considered. The grading of the mesh is done using simple-grading, and there was no refinement of the mesh carried out (refer Fig. 4.1 and Appendix). Accordingly, the mesh constitutes around 100300 cells and shown in Fig. 4.2.

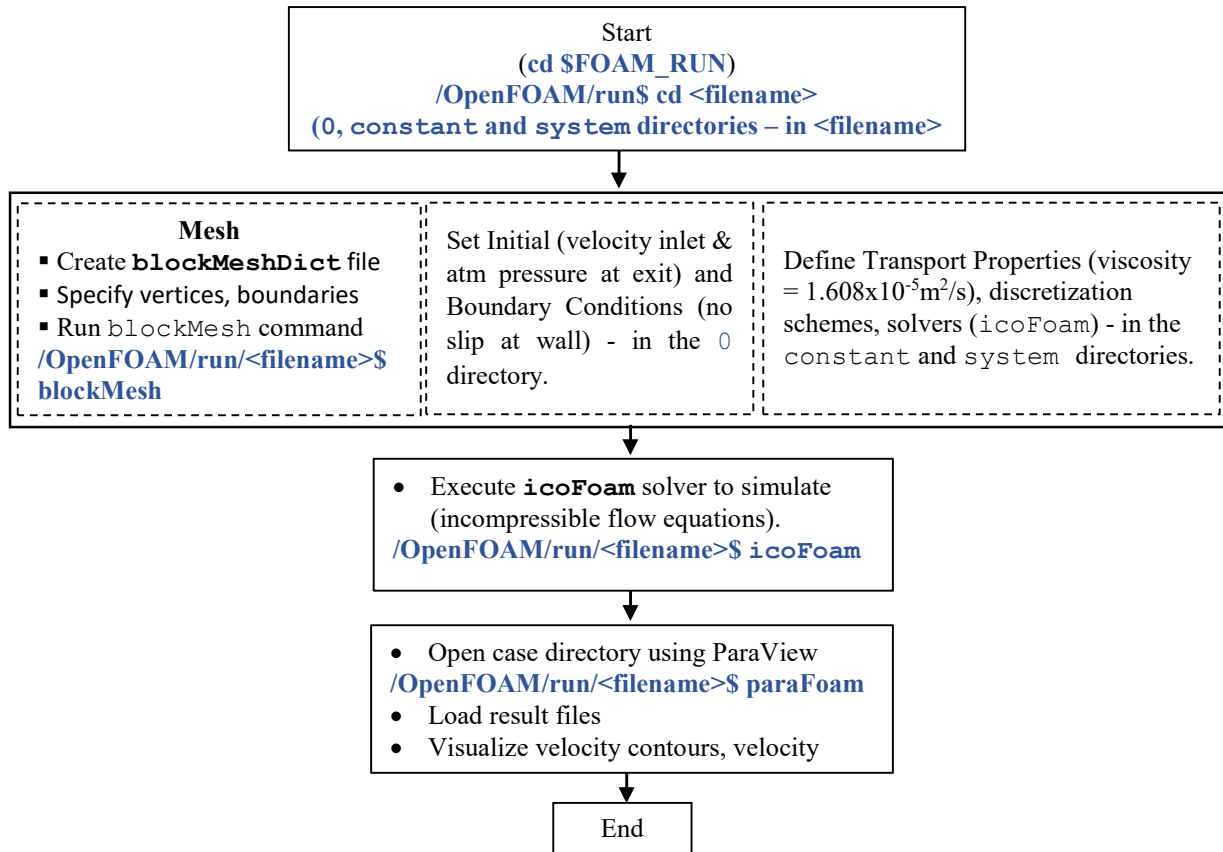


Fig. 4.1 Procedure to simulate using OpenFOAM

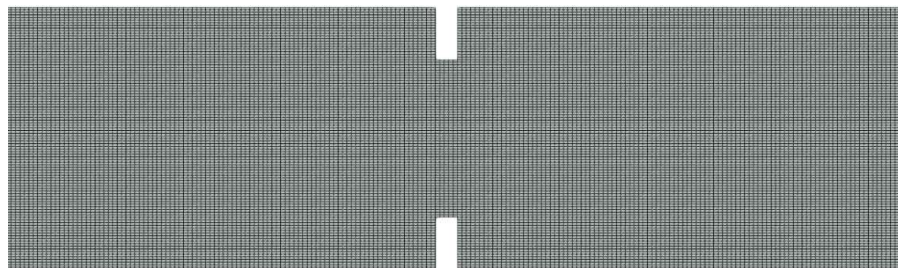


Fig. 4.2 Generated mesh

## 4.2 Initial and Boundary Conditions

In the present analysis, all the surfaces are considered as “no-slip” except the inlet and the outlet. The inlet is velocity inlet with a constant velocity and the outlet is pressure outlet with atmospheric (zero gauge pressure) is considered. Accordingly, the boundary conditions are indicated as field files such as *p*, *U*, in time directories. In the present analysis, the pressure is defined as kinematic pressure ( $\text{m}^2/\text{s}^2$ ), which is the pressure divided by the density of the fluid. These files constitute three entities - dimensions, internalField and the boundaryField. In the geometry field, the dimensional units are specified, in the internalField initial values are provided

**Table 4.1** Details of Boundary conditions

	<b>P</b>	<b>U</b>
Inlet	zeroGradient	fixedValue; inletValue (present case(s): 0.0032m/s, 0.016m/s and 0.032m/s)
Outlet	fixedValue; uniform 0 (zero gauge pressure)	inletOutlet
Fixedwall	zeroGradient	noSlip
ContactWall1	zeroGradient	noSlip
ContactWall2	zeroGradient	noSlip
frontAndBack	empty	empty

and boundary conditions are indicated in the boundaryField. These boundary conditions are provided as patches (refer Appendix). As indicated in the preceding sections, the flow is laminar for all the three cases of Reynolds number considered in the present analysis. Further, the simulations are carried out for times steps of 0.05sec for a period of 20sec, and thus resulting in the Courant number ( $Co=U\Delta t/\Delta x$ ) of  $Co < 1$  for all the cases.

### 4.3 Solver

In the present analysis, icoFoam solver is employed. IcoFoam is a transient analysis solver that may be employed for incompressible, laminar flow of Newtonian fluids. The PISO algorithm is employed for the solution. The solution is attained employing the default Euler supported by Gauss Linear and orthogonal. As a convergence criteria, the residual values of  $10^{-6}$  for pressure and  $10^{-5}$  for velocity are considered.

## 5. Results and Discussions

### 5.1 Validation of simulated results

Also, it was demonstrated by Tu et al. (2006) that the characteristics of the flow with partial blockages (considering as orifice) may be described using the following dimensionless parameters.

$$f\left(\frac{l}{d}, \frac{d}{D}, Re, Eu, C_d\right) \quad (3)$$

where  $l$ ,  $d$  and  $D$  refers to thickness of blockage, diameter of blockage opening and diameter of pipe. The  $Re$ ,  $Eu$  and  $C_d$  indicates the Reynolds number, Euler's number and Coefficient of discharge.

$$Re = \frac{\rho U D}{\mu} \quad (4)$$

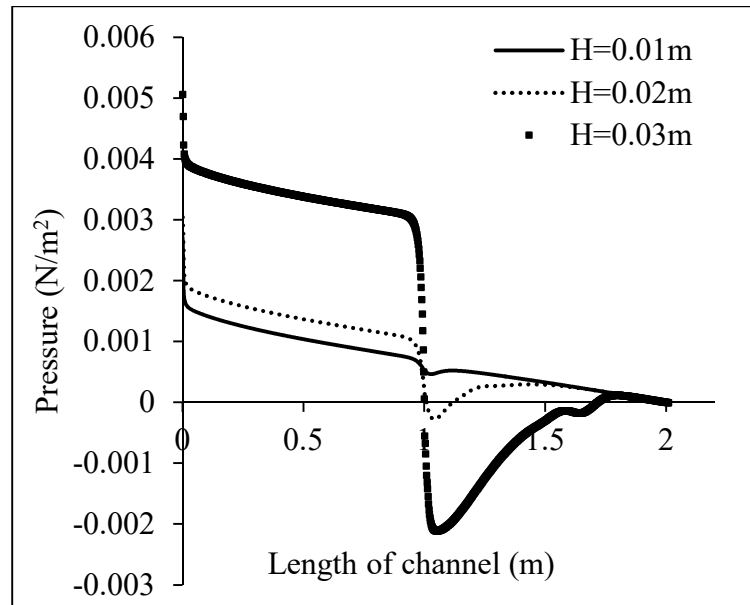
$$Eu = \frac{2 \Delta P d^4}{\rho U^2 D^4} \quad (5)$$

$$C_d = \frac{U}{d^4} D^4 \sqrt{\rho \frac{(1 - (\frac{d}{D})^4)}{2 \Delta P}} \quad (6)$$

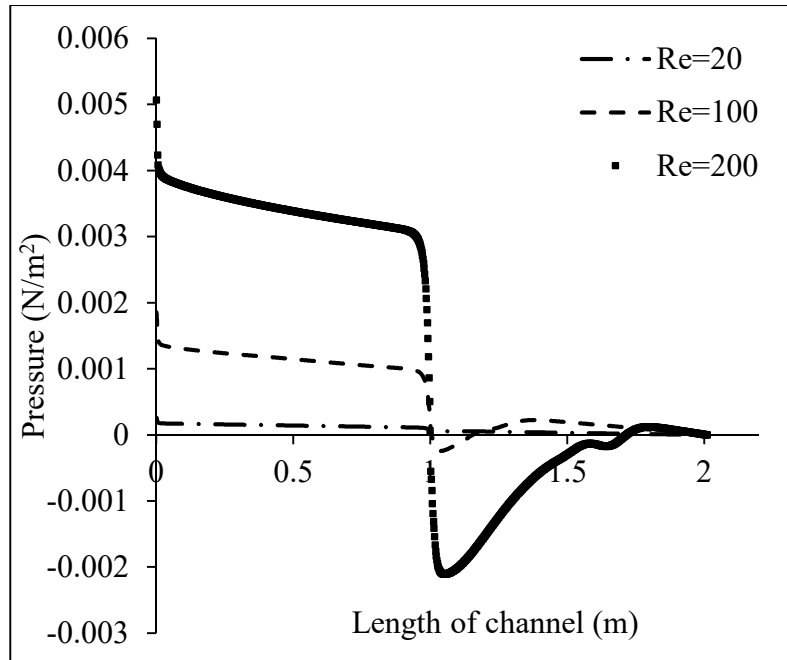
Accordingly, for the present analysis, employing these dimensionless parameters, the validation of the simulated results is carried out. For a case of  $Re=100$ ,  $l/d=0.17$  and  $d/D=0.6$ , the value of coefficient of discharge  $C_d$  is found to be 0.81. Though exact flow condition is not available in the literature, a proximate flow condition of  $Re=100$ ,  $l/d=0.125$  and  $d/D=0.5$  of experimental data of Sahin & Ceyhan (1996), the  $C_d$  value was documented as 0.7. The observed  $C_d$  value constitutes approximately 12% of deviation in pressure gradient.

## 5.2 Pressure gradient across the flow

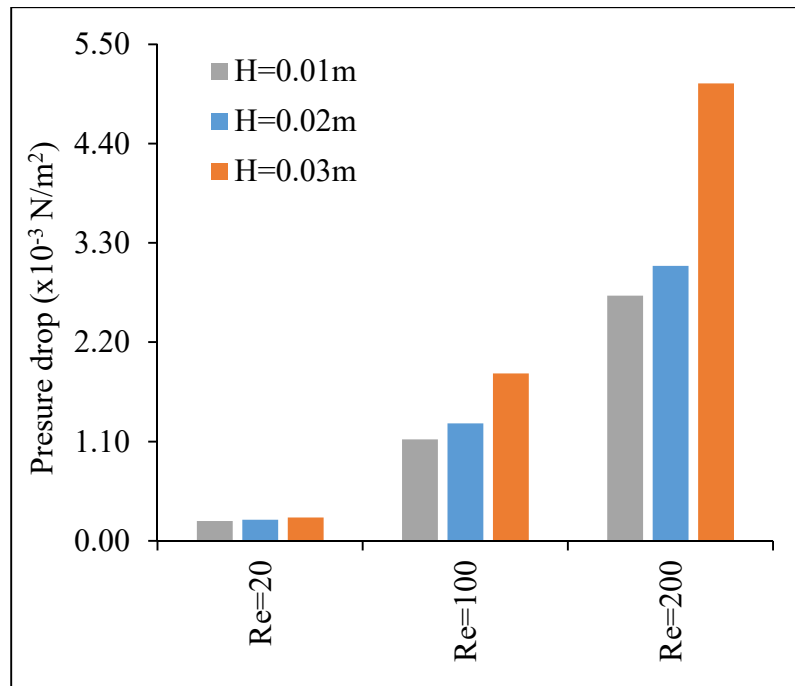
The pressure characteristics across the flow for various Reynolds number and span of constriction is described below (Fig. 5.1 and Fig. 5.2). The Fig. 5.1 indicates the pressure



**Fig. 5.1** Pressure variation along the flow with constrictions ( $Re=200$ )

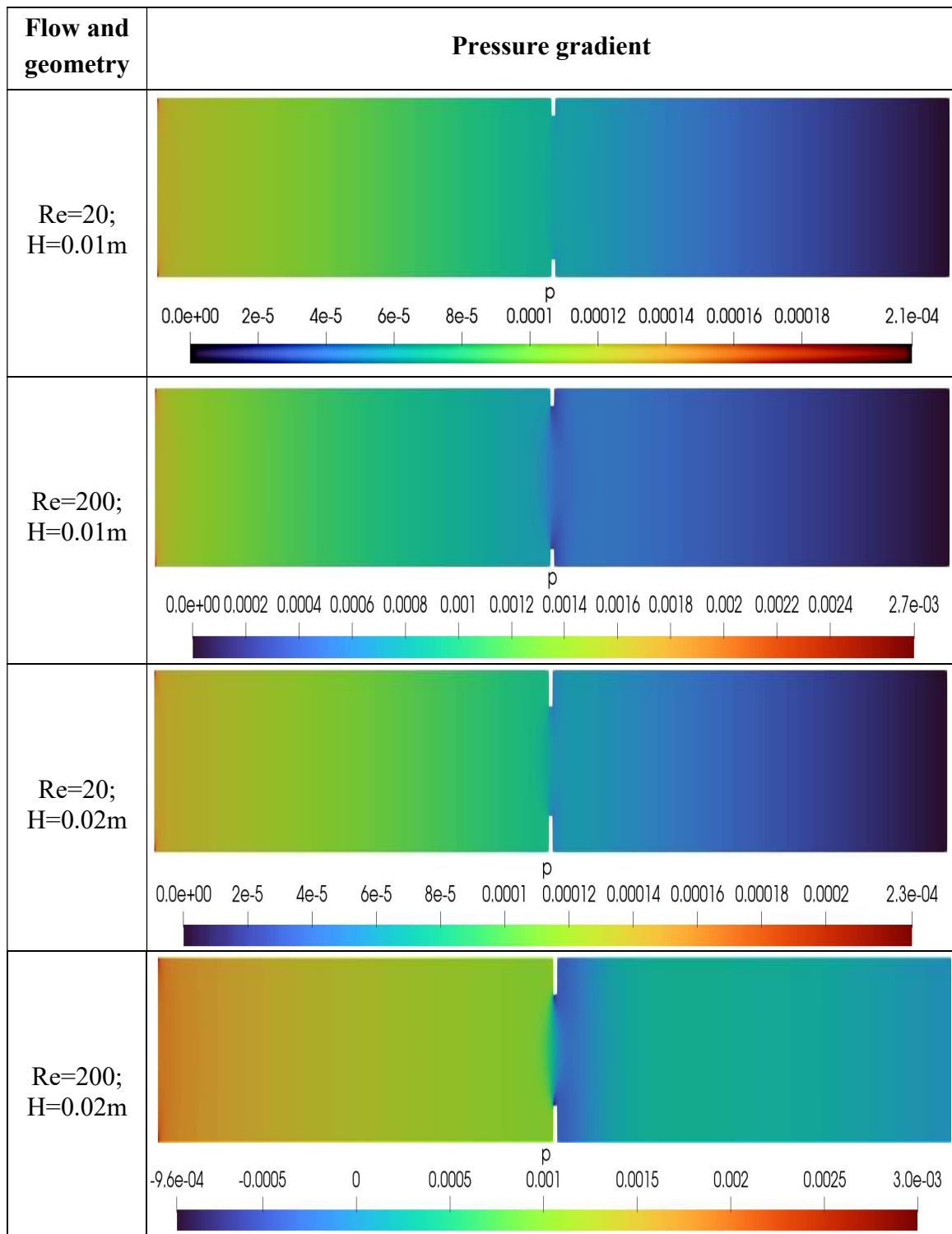


**Fig. 5.2** Pressure variation along the flow with constriction ( $H=0.03\text{m}$ )

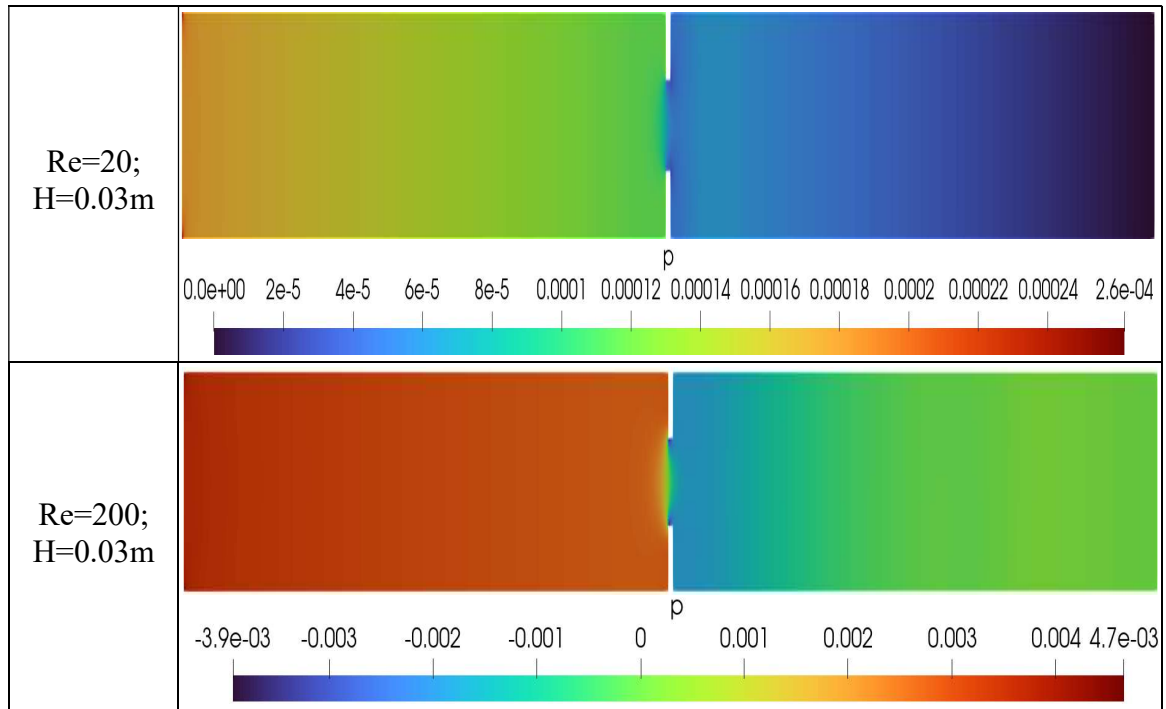


**Fig. 5.3** Pressure gradient for different flow conditions

variation for various constriction spans for a Reynolds number of 200. However, Fig.5.2 shows the pressure variation for different Reynolds number at constriction span of  $H=0.03\text{m}$ . From these figures, it may be observed that the pressure drop at the constriction is increases with Reynolds number and span of the constriction. Further, the pressure drop across the flow for various flow conditions are given in Fig. 5.3. The figure clearly indicates that with increasing Reynolds number and with increasing constriction sizes.

**Table 5.1** Pressure gradient for various flow conditions





The pressure contours for different flow conditions are plotted (Table 5.1 above). From the pressure contours, for smaller Reynolds number ( $Re=20$ ) and smaller constrictions ( $H=0.01m$ ), the variation in pressure across the constriction is smooth. However, with increasing Reynolds number and constriction size, there is considerable build-up of pressure upstream of constriction with simultaneous and significant pressure drop downstream of constriction. Such a kind of phenomenon are noted to be critical in many industrial applications (Gong et al. 2014).

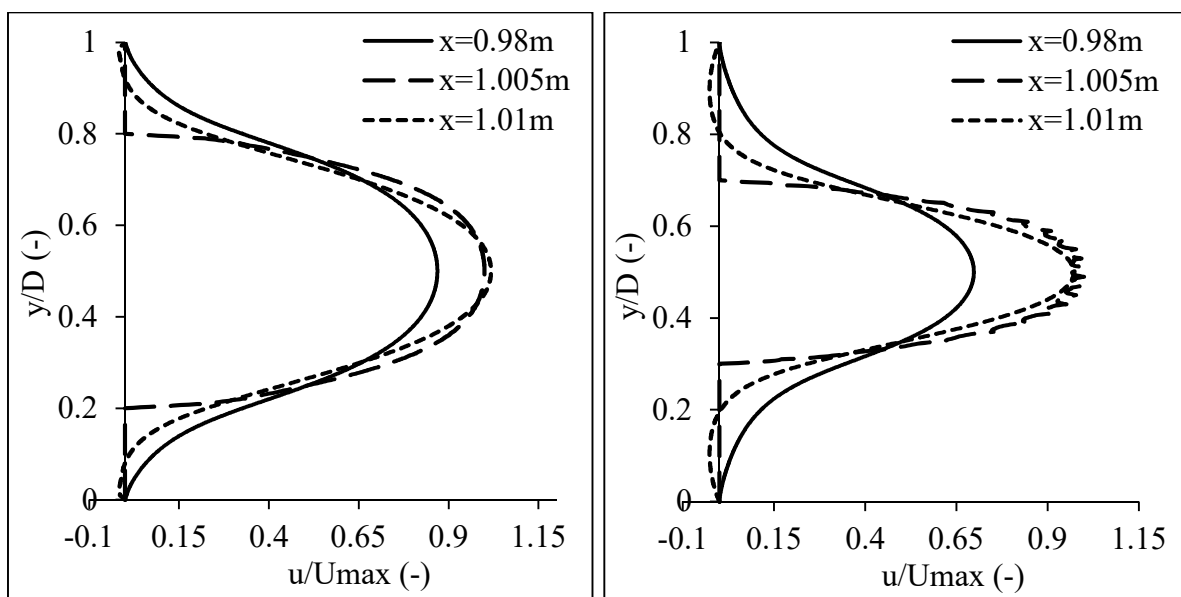


Fig. 5.4a and Fig. 5.4b Velocity profile ( $Re = 20$ ;  $H=0.02m$  and  $Re=20$ ;  $H=0.03m$ )

### 5.3 Flow characteristics

The numerical results of velocity characteristics of the air flow through the 2D channel are described below. The velocity profile is non-dimensionalized using the maximum velocity of the flow. The maximum velocity, as expected is observed at the insert. Accordingly, the cross

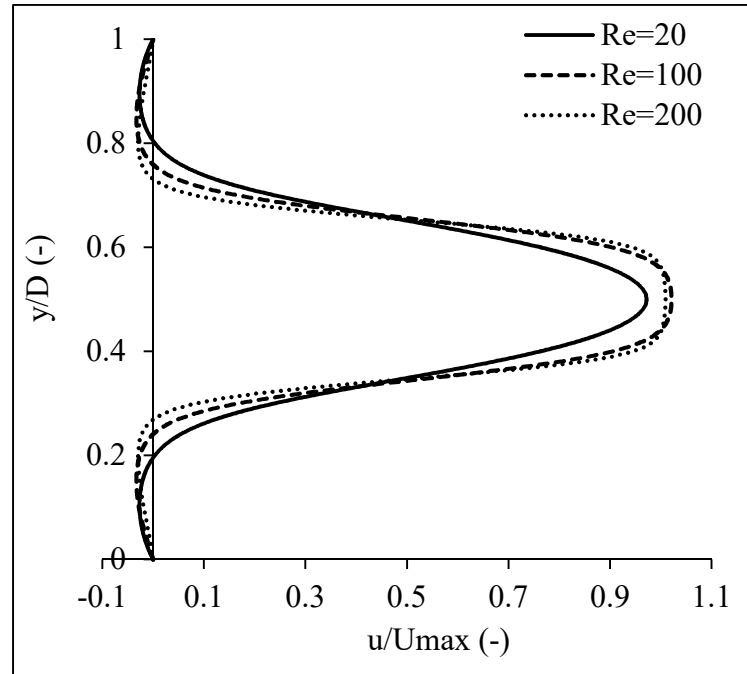


Fig. 5.5 Velocity profile across flow cross-section ( $H=0.03\text{m}$ )

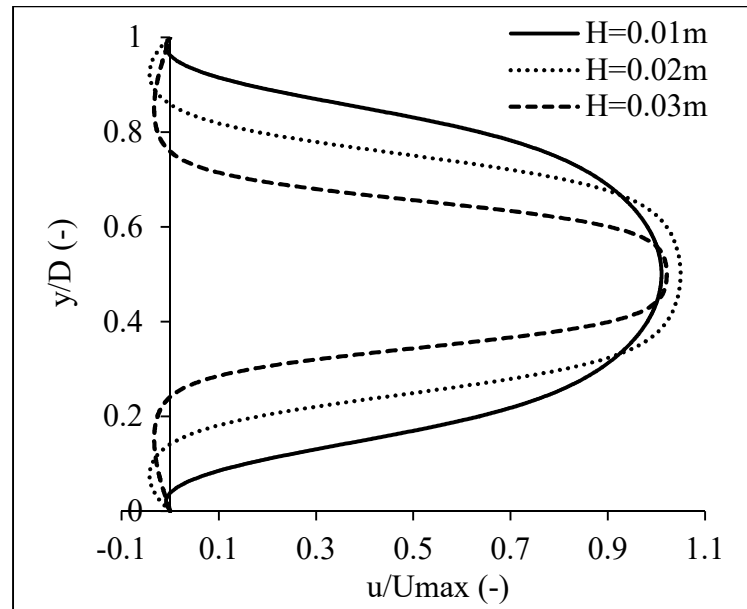


Fig. 5.6 Velocity profile across flow cross-section ( $\text{Re}=100$ )

section is non-dimensionalized using the width of the channel ( $D = 0.1\text{m}$ ). The figures Fig. 5.4a and Fig. 5.4b indicates the velocity profiles at three cross sections across the flow for  $\text{Re}=20$ ;  $H=0.02$  and  $\text{Re}=200$ ;  $H=0.03\text{m}$  respectively. The three cross sections shown in the figures are

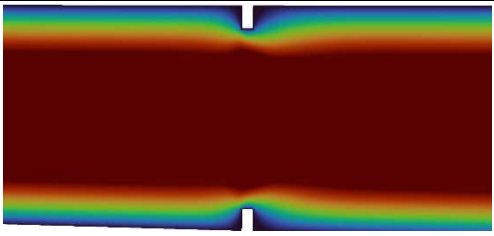
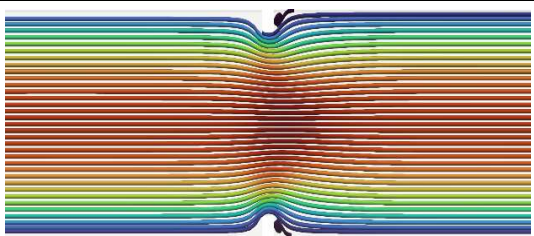
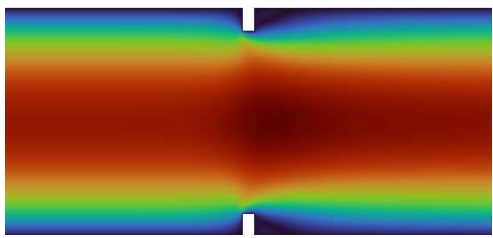
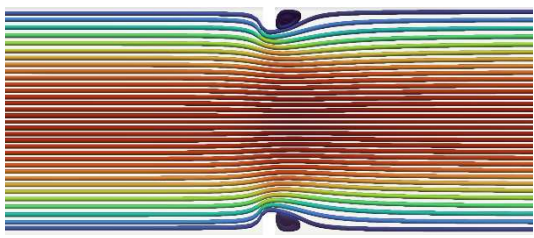
just before the constriction ( $x=0.98\text{m}$ ), at the centre of the constriction ( $x=1.005\text{m}$ ) and immediately after the constriction ( $x=1.01\text{m}$ ) respectively. From the figures, it is observed that the velocity profiles at the upstream and the downstream vary with the increase in the constriction size.

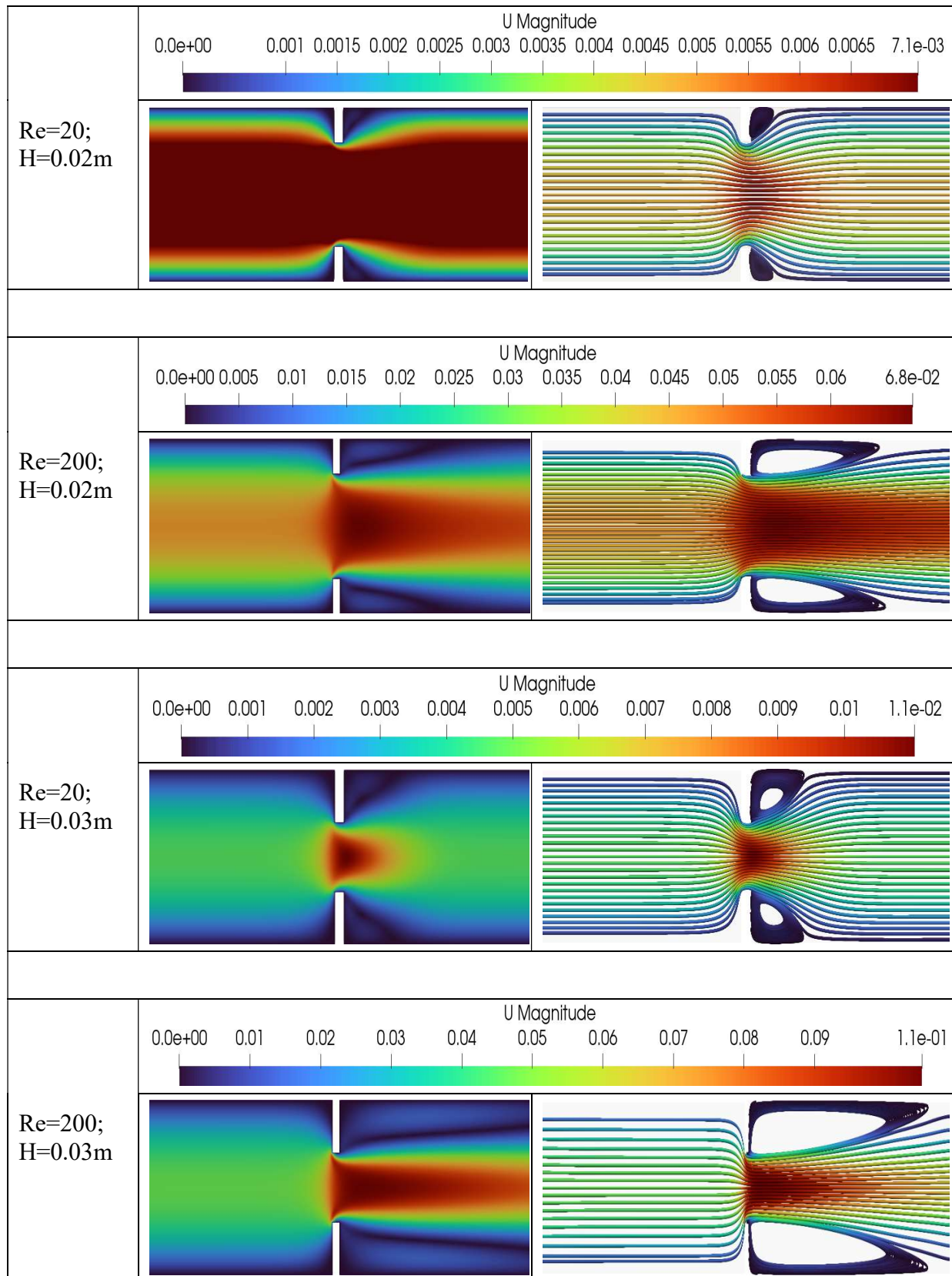
Further, to evaluate the effect of Reynolds number variation, the velocity profiles downstream of constriction with constriction size ( $H=0.03\text{m}$ ) is plotted for different Reynolds number (Fig. 5.5 above). Similarly, for a given flow ( $Re=200$ ), for various constriction sizes, the velocity profiles downstream of the constriction is given in Fig. 5.6. From these figures (Fig. 5.5 and Fig. 5.6), it may be noted that the velocity increases at higher constriction size of  $H=0.03\text{m}$  compared to the other constriction sizes of  $H=0.01\text{m}$  and  $H=0.02\text{m}$ . Also, the shape of the velocity profile is found to be broad at higher Reynolds number.

#### 5.4 Recirculation zones:

From the velocity profiles described above, there are recirculation zones observed at higher constriction sizes and higher Reynolds number. Accordingly, to analyse the evolution of recirculation zones across the flow, the velocity stream lines are shown in Table 5.2 below.

Table 5.2 Velocity streamlines

Flow and geometry	Velocity contours	Velocity stream lines
Re=20; H=0.01m	U Magnitude 0.0e+00 0.0005 0.001 0.0015 0.002 0.0025 0.003 0.0035 0.004 0.0045 0.005 5.4e-03	
		
Re=200; H=0.01m	U Magnitude 0.0e+00 0.005 0.01 0.015 0.02 0.025 0.03 0.035 0.04 0.045 5.1e-02	
		



## 6. Conclusions

The CFD simulations of the 2D air flow through a channel with constriction using icoFoam solver of OpenFOAM. The simulation results were validated using the experimental work available in

the literature. The Reynolds number was varied as  $Re = 20, 100$  and  $200$ . The constriction size was also varied from  $H=0.01\text{m}$ ,  $0.02\text{m}$  and  $0.03\text{m}$ . The velocity and pressure characteristics were analysed. From the analysis, the significant observations are as follows:

1. With the increase in the span of the constriction, the pressure gradient increases. This increase in the pressure gradient with the increase in the span of constriction is found to be substantial at higher Reynolds number.
2. The velocity streamlines indicate the recirculation zones, in particular downstream of the constriction. The size of recirculation zones found to increase with Reynolds number and constriction size.

## References

1. Covas, D., Meniconi, S., Capponi, C., & Brunone, B. (2023). Hydrodynamics of laminar pipe flow through an extended partial blockage by CFD, *Journal of Hydroinformatics*, 00(1), doi: 10.2166/hydro.2023.042
2. Ferrante, M., Brunone, B., Meniconi, S., Karney, B. W., & Massari, C. (2014). Leak size, detectability and test conditions in pressurized pipe systems. *Water Resources Management* 28, 4583–4598. doi:10.1007/s11269-014-0752-6.
3. Gong, J., Lambert, M. F., Simpson, A. R. & Zecchin, A. C. (2014). Detection of localized deterioration distributed along single pipelines by reconstructive MOC analysis. *Journal of Hydraulic Engineering* 140, 190–198. doi:10.1061/(asce)hy. 1943-7900.0000806.
4. Hasegawa, T., Suganuma, M. & Watanabe, H. (1997). Anomaly of excess pressure drops of the flow through very small orifices. *Physics of Fluids* 9 (1), 1–3
5. Johansen, F. C. (1997). Flow through pipe orifices at low Reynolds numbers. *Proceedings of the Royal Society of London. Series A*, 126 (801), 231–245.
6. Keramat, A., Wang, X., Louati, M., Meniconi, S., Brunone, B. & Ghidaoui, M. S. (2019). Objective functions for transient-based pipeline leakage detection in a noisy environment: Least square and matched-filter. *Journal of Water Resources Planning and Management* 145 (10), 04019042.
7. Kiljanski, T. (1993). Discharge coefficient for free jets from orifices at low Reynolds number. *ASME Journal of Fluids Engineering*, 115 (4), 778–781.
8. Martins, N. M. C., Covas, D. I. C., Meniconi, S., Capponi, C. & Brunone, B. (2021). Characterisation of low-Reynolds number flow through an orifice: CFD results vs. laboratory data. *Journal of Hydroinformatics* 23 (4), 709–723.
9. Meniconi, S., Brunone, B., Ferrante, M. & Capponi, C. (2016). Mechanism of interaction of pressure waves at a discrete partial blockage. *Journal of Fluids and Structures*, 62, 33–45.
10. Papadopoulou, K. A., Shamout, M. N., Lennox, B., Mackay, D., Taylor, A. R., Turner, J. T. & Wang, X. (2008). An evaluation of acoustic reflectometry for leakage and blockage detection. *Proceedings of the Institution of Mechanical Engineers. Part C: Journal of Mechanical Engineering Science*, 222 (6), 959–966.
11. Sahin, B. & Ceyhan, H. (1996). Numerical and experimental analysis of laminar flow through square-edged orifice with variable thickness. *Transactions of the Institute of Measurement and Control* 18 (4), 166–174.
12. Tu, X., Hrnjak, P. S. & Bullard, C. W. (2006). Refrigerant 134a liquid flow through micro-scale short tube orifices with/without phase change. *Experimental Thermal and Fluid Science*, 30 (3), 253–262.

13. Yang, L., Fu, H., Liang, H., Wang, Y., Han, G. & Ling, K. (2019). Detection of pipeline blockage using lab experiment and computational fluid dynamic simulation. *Journal of Petroleum Science and Engineering* 183, 106421–106410.
14. Zhou, D., Karatayev, K., Fan, Y., Straiton, B., & Marashdeh, Q. (2024). Experimental Study of Oil–Water Flow Downstream of a Restriction in a Horizontal Pipe. *Fluids*, 9 (146), <https://doi.org/10.3390/fluids9060146>.

## Appendix

```

/*-----*- C++ -*-----*\
=====
\ \ / F i e l d | OpenFOAM: The Open Source CFD Toolbox
\ \ / O p e r a t i o n | Website: https://openfoam.org
\ \ / A n d | Version: 12
\ \ M a n i p u l a t i o n |
\*-----*/

FoamFile
{
    format    ascii;
    class     dictionary;
    object    blockMeshDict;
}
// ***** //

convertToMeters 1;

vertices
(
    (0 0 0) //0
    (1 0 0) //1
    (1 0.1 0) //2
    (0 0.1 0) //3
    (1 0.03 0) //4
    (1.01 0.03 0) //5
    (1.01 0.07 0) //6
    (1 0.07 0) //7
    (1.01 0 0) //8
    (2.01 0 0) //9
    (2.01 0.1 0) //10
    (1.01 0.1 0) //11

    (0 0 0.01) //12
    (1 0 0.01) //13
    (1 0.1 0.01) //14
    (0 0.1 0.01) //15
    (1 0.03 0.01) //16
    (1.01 0.03 0.01) //17
    (1.01 0.07 0.01) //18
    (1 0.07 0.01) //19
    (1.01 0 0.01) //20
    (2.01 0 0.01) //21

```

```

(2.01 0.1 0.01) //22
(1.01 0.1 0.01) //23s
);

blocks
(
  hex (0 1 2 3 12 13 14 15) (500 100 1) simpleGrading (1 1 1)
  hex (4 5 6 7 16 17 18 19) (1 60 1) simpleGrading (1 1 1)
  hex (8 9 10 11 20 21 22 23) (500 100 1) simpleGrading (1 1 1)
);

boundary
(
  inlet
  {
    type patch;
    faces
    (
      (0 12 15 3)
    );
  }
  outlet
  {
    type patch;
    faces
    (
      (9 21 22 10)
    );
  }
  Fixedwall
  {
    type wall;
    faces
    (
      (2 3 15 14)
      (1 0 12 13)
      (10 11 23 22)
      (9 8 20 21)
      (6 7 19 18)
      (5 4 16 17)
    );
  }
}

```



```

ContactWall1
{
    type wall;
    faces
    (
        (2 1 13 14)
        (11 8 20 23)
    );
}

ContactWall2
{
    type wall;
    faces
    (
        (7 4 16 19)
        (6 5 17 18)
    );
}

frontAndBack
{
    type empty;
    faces
    (
        (0 1 2 3)
        (12 13 14 15)
        (4 5 6 7)
        (16 17 18 19)
        (8 9 10 11)
        (20 21 22 23)
    );
}

);

mergePatchPairs
(
    (ContactWall2 ContactWall1)
);

// *****

/*-----*- C++ -*-----*\
=====
\  / Field | OpenFOAM: The Open Source CFD Toolbox

```

```

\\ / O peration | Website: https://openfoam.org
\\ / A nd      | Version: 12
\\ \ M anipulation |
\*-----*/
FoamFile
{
    format    ascii;
    class     dictionary;
    location  "system";
    object    controlDict;
}
// *****
application  icoFoam;

startFrom    startTime;

startTime    0;

stopAt       endTime;

endTime      20;

deltaT       0.5;

writeControl  timeStep;

writeInterval 20;

purgeWrite   0;

writeFormat   ascii;

writePrecision 6;

writeCompression off;

timeFormat    general;

timePrecision 6;

runTimeModifiable true;

```

```
// *****

/*-----*- C++ -*-----*\
=====
\\  / F ield      | OpenFOAM: The Open Source CFD Toolbox
\\  / O peration  | Website: https://openfoam.org
\\  / A nd        | Version: 12
\\  / M anipulation |
\*-----*/

FoamFile
{
    format    ascii;
    class     dictionary;
    location  "system";
    object    fvSchemes;
}
// *****

ddtSchemes
{
    default    Euler;
}

gradSchemes
{
    default    Gauss linear;
    grad(p)    Gauss linear;
}

divSchemes
{
    default    none;
    div(phi,U) Gauss linear;
}

laplacianSchemes
{
    default    Gauss linear orthogonal;
}

interpolationSchemes
{
    default    linear;
}

snGradSchemes
{
    default    orthogonal;
}
```

```

}
// *****

/*-----*- C++ -*-----*\
=====
\ \ / F ield      | OpenFOAM: The Open Source CFD Toolbox
\ \ / O peration  | Website: https://openfoam.org
\ \ / A nd        | Version: 12
\ \ M anipulation |
\*-----*/

FoamFile
{
    format    ascii;
    class     dictionary;
    location  "system";
    object    fvSolution;
}
// *****

solvers
{
    p
    {
        solver      PCG;
        preconditioner DIC;
        tolerance    1e-06;
        relTol       0.05;
    }
    pFinal
    {
        $p;
        relTol       0;
    }
    U
    {
        solver      smoothSolver;
        smoother     symGaussSeidel;
        tolerance    1e-05;
        relTol       0;
    }
}

PISO
{

```

```
nCorrectors    2;
nNonOrthogonalCorrectors 0;
pRefCell       0;
pRefValue      0;
}
// ***** //
```